Advances in Fluid, Heat and Materials Engineering

Journal homepage:
https://karyailham.com.my/index.php/afhme/index
ISSN: 3083-8134

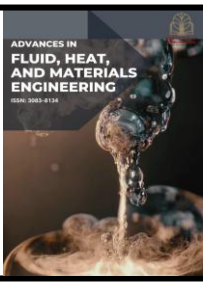

Numerical Study of Incompressible Flow Through a Pipe with an Orifice Constriction Using Ansys Fluent

Yashlen Pichyalagan[1,*]

[1] Faculty of Mechanical and Manufacturing Engineering, Universiti Tun Hussein Onn Malaysia, 86400 Parit Raja, Johor, Malaysia

ARTICLE INFO

Article history:
Received 13 December 2025
Received in revised form 12 January 2026
Accepted 6 February 2026
Available online 31 March 2026

Keywords:
Computational Fluid Dynamics (CFD); incompressible flow; orifice contraction; mesh independence; Reynolds number; turbulence models; pressure drop; velocity distribution

ABSTRACT

Incompressible flows with sudden contractions, such as those created by orifice plates, exhibit complex behaviour including flow acceleration, pressure losses, and downstream separation. Predicting these features accurately remains challenging due to the sensitivity of CFD results to mesh resolution, flow regime, and turbulence modelling. This study investigates how mesh quality, Reynolds number variation, and turbulence model selection influence pressure and velocity predictions in a pipe containing an orifice contraction. Results indicate that mesh refinement improves accuracy, with minimal benefit beyond the medium mesh. Increasing the Reynolds number substantially alters flow behaviour, with the inlet pressure rising by approximately 9.5% from laminar to transitional conditions, while the pressure difference in the turbulent regime becomes about 52% lower than in the transitional regime. Among the turbulence models tested, the Realizable k-ε and k-ω SST models show better agreement with expected separation patterns compared to the Standard k-ε. Overall, the findings highlight the importance of mesh selection, flow regime characterisation, and turbulence modelling in achieving reliable CFD predictions for orifice-induced pipe flow.

1. Introduction

A basic fluid mechanics problem that frequently arises in piping systems, pressure-reducing components, metering devices, and industrial equipment is the flow through a pipe with an abrupt contraction or orifice plate [1]. To guarantee system efficiency and safety, it is necessary to precisely estimate the acceleration, flow separation, and pressure losses caused by the geometric discontinuity. An effective method for analysing such flows without requiring complex experimental setups is computational fluid dynamics, or CFD. However, mesh resolution, turbulence modelling, and flow regime selection have a significant impact on CFD accuracy [2]. The goal of this research is to use ANSYS Fluent to conduct a thorough parametric study of these factors. Because these geometries produce severe velocity gradients, large pressure losses, and intricate flow patterns, flow through pipes with abrupt contractions or orifice-type constraints has been thoroughly researched.

---

[*] *Corresponding author.*
E-mail address: dd220022@student.uthm.edu.my

https://doi.org/10.37934/afhme.8.1.1023a

Subsequently, fluid accelerates rapidly as it travels through an aperture, creating a vena contracta and downstream recirculation zones [3]. The behaviour of these distinct shear layers and vortices, which cause irreversible head loss, is highly dependent on the Reynolds number, area ratio, and boundary layer development. Although traditional experimental research has shed light on pressure drop characteristics, their inability to capture intricate flow structures has sparked interest in numerical methods [4]. Because it can resolve velocity fields, pressure distributions, and turbulence features with great spatial resolution, computational fluid dynamics (CFD) has emerged as a useful tool for analysing orifice flows. However, the choice of turbulence model and mesh refinement have a significant impact on CFD accuracy. While fine meshes enhance resolution at the contraction and jet regions, coarse meshes usually smear velocity gradients as seen in [5].

Furthermore, different turbulence models operate differently. The Realizable k-ε and k-ωSST models provide better forecasts for shear layers and unfavourable pressure gradients, whereas the Standard k-ε model frequently has trouble with flow separation. The current study on flow through a pipe with an orifice contraction using ANSYS Fluent is based on these earlier research findings, which emphasize the significance of mesh quality, flow regime, and turbulence modelling.

2. Methodology

2.1 Geometry of Pipe with Orifice

This section examines how different pipe shapes affect the flow characteristics. Three designs were taken into consideration, all of which kept the pipe's overall length at 300 mm and placed the orifice at its midpoint (150 mm) as shown in Figure 1. Table 1 shows the design specifications in order to evaluate how constriction ratios affect velocity and pressure distributions; the geometries have different input and exit sizes. Design 1 has the greatest cross-sectional area of the three, with an inlet diameter (D1) of 100 mm and an output diameter (D2) of 50 mm. With D1 at 75 mm and D2 at 37.5 mm, Design 2 reduces the diameters proportionately. With D1 measuring 50 mm and D2 measuring 25 mm, Design 3 Is the smallest configuration. In order to provide insight into the best design considerations for attaining required velocity and pressure performance, the analysis compares different geometries in order to show the relationship between pipe diameter reduction, flow acceleration through the orifice, and consequent pressure changes.

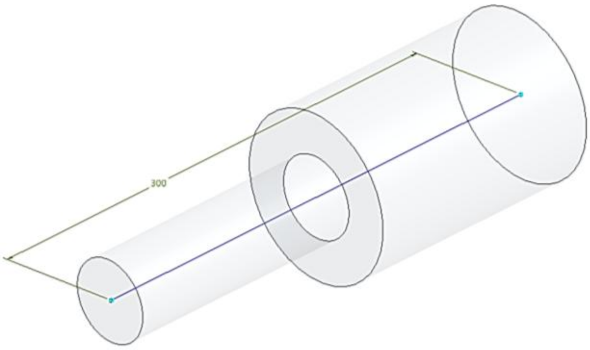

Fig. 1. Geometry size

Table 1
Geometry dimension variation

Designs	Diameter 1 (mm)	Diameter 2 (mm)	Length (mm)
Design 1	8.213	37.10	300
Design 2	7.819	36.32	300
Design 3	8.496	41.13	300

2.2 Discretization

2.2.1 Mesh

A hexahedral mesh was developed for the circular pipe containing the orifice contraction to ensure accurate resolution of the flow behaviour under incompressible conditions as shown in Table 2. The mesh was refined in critical regions such as the sharp edges of the orifice and the downstream recirculation zone, where strong gradients in velocity and pressure are expected. Hexahedral elements were chosen because they provide better numerical stability and lower interpolation errors for internal flow simulations. This meshing approach ensured that the simulation could capture the geometric complexity of the contraction while maintaining consistent accuracy throughout the domain.

In order to simulate internal pipe flow under stable conditions, boundary conditions were used, as shown in Figure 2. Three separate intake velocities were assigned to create three different Reynolds numbers, which represented laminar, transitional, and turbulent regimes. The inlet was described as a velocity inlet. The solver was able to modify the exit velocity according to internal flow development since the outlet was designated as a pressure outlet with a gauge pressure of 0 Pa. To accurately simulate viscous effects along the boundary layer, the pipe walls were regarded as fixed no-slip boundaries. The working fluid was atmospheric air, and throughout the simulation, it was assumed that the flow was incompressible.

Table 2
Mesh Information

Model	Coarse mesh		Medium mesh		Fine mesh	
	Nodes	Elements	Nodes	Elements	Nodes	Elements
1	4364	3801	5606	4864	22760	20032

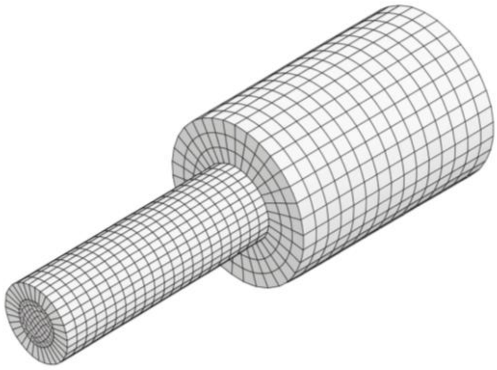

Fig. 2. Hexa mesh

2.2.2 Grid independency test

In order to conduct a grid independence study, three computational grids, coarse, medium, and fine were built using ANSYS Meshing. The global topology of all three meshes remained the same, but their element counts and levels of fineness varied. Near the contraction zone, where sharp velocity gradients and flow separation were anticipated, the mesh was gradually improved. To increase numerical accuracy and reduce skewness, particularly along the pipe walls and at the contraction throat, a structured mesh was utilized whenever feasible. To ensure that discretization mistakes had no effect on flow forecasts, the grid independence test was crucial (Table 3).

Table 3
Geometry dimension variation

Mesh type	Number of nodes	Number of elements
Coarse	8.213	37.10
Medium	7.819	36.32
Fine	8.496	41.13

2.2.3 Turbulence models

Three turbulence models as shown in Figure 2 were used to assess the impact of turbulence modelling: the Standard k-ε, the Realizable k-ε, and the k-ωSST model. Every model was run for every mesh density and Reynolds number. The SIMPLE approach for pressure - velocity coupling was utilized in conjunction with ANSYS Fluent's pressure-based solver. To reduce numerical diffusion, particularly in the vicinity of the contraction, second-order spatial discretization schemes were used. By keeping an eye on residuals until they dropped below 10-5 and making sure that important variables, such the mass flow rate at the outlet and the pressure drop over the contraction, attained steady values, convergence was evaluated.

Lastly, for every simulated example, post-processing was done to obtain centreline profiles, pressure contours, and velocity contours. Comparing the pressure drop and maximum velocity at the contraction between the three meshes was the main method used to assess the grid independence study. In the meantime, the prediction of flow separation, recirculation zones downstream of the contraction, and peak velocity magnitude at the throat were used to evaluate the performance of the turbulence model.

2.2.4 Reynolds numbers

Three different types of flow, laminar, transitional and turbulent flows were tested against the pipe with orifice constriction to analyze the velocity and pressure difference that has been created due to these differences. The Reynolds number was calculated to characterise the flow regime inside the pipe and to determine the behaviour of the fluid for the cases created in this study. The Reynolds number is defined as:

$$\mathrm{Re} = \frac{\rho \mathrm{VD}}{\mu} \tag{1}$$

where $\rho$is the fluid density, $\mathrm{V}$is the average flow velocity, $\mathrm{D}$is the characteristic diameter, and $\mu$is the dynamic viscosity [6].

Three Reynolds numbers were deliberately chosen and implemented as separate simulation cases by the authors to represent laminar, transitional and turbulent flow conditions in the orifice pipe design. The laminar case examines flow dominated by viscous effects, the transitional case captures the onset of instabilities and mixed behaviour, and the turbulent case investigates flow where inertial effects and turbulence dominate. Comparing these three controlled cases allows direct assessment of how flow regime influences velocity acceleration, separation and pressure variation across the orifice, and it validates the suitability of the turbulence modelling strategies applied in subsequent analyses [7].

2.3 Governing Equations

The flow inside the pipe and through the orifice is assumed to be incompressible, steady, and Newtonian. Under these conditions, the fluid behaviour is described by the conservation laws of mass and momentum. These equations form the basis of the numerical solution implemented in the CFD solver. The conservation of mass, also known as the continuity equation for incompressible flow, ensures that the velocity field satisfies the requirement of constant fluid density throughout the domain. It is expressed as:

$$\nabla \cdot \vec{u} = 0 \tag{2}$$

where $\vec{u}$is the velocity vector. This equation enforces that no accumulation or depletion of mass occurs within any control volume [8].

The conservation of momentum is governed by the incompressible Navier Stokes equations. These equations account for the balance between inertial forces, pressure forces, and viscous stresses acting on the fluid. The momentum equation is written as:

$$\rho(\vec{u} \cdot \nabla\vec{u}) = -\nabla p + \mu\nabla^2\vec{u} \tag{3}$$

where $\rho$is the fluid density, $p$is the static pressure, and $\mu$is the dynamic viscosity of the fluid. The pressure gradient term represents the driving force that accelerates the fluid, while the viscous term accounts for internal resistance to deformation [9].

For cases involving higher Reynolds numbers, the flow may transition to turbulence downstream of the orifice. In such conditions, the instantaneous velocity field contains fluctuating components that require time averaging. This leads to the use of the Reynolds Averaged Navier Stokes (RANS) formulation, which introduces the Reynolds stress term to represent the effect of turbulent fluctuations. The RANS form of the momentum equation is expressed as:

$$\rho\left(\vec{U} \cdot \nabla\vec{U}\right) = -\nabla P + \mu\nabla^2\vec{U} - \nabla \cdot \left(\rho u_{\imath}{}'\bar{u}_{\jmath}{}'\right) \tag{4}$$

where $\vec{\mathrm{U}}$ is the mean velocity. These stresses require closure through a suitable turbulence model, which is addressed in a later section.

The governing equations above form the mathematical foundation of all simulations conducted in this study. They describe the motion of the fluid under steady, incompressible conditions and are solved numerically to obtain predictions of velocity, pressure distribution, and flow behaviour near the orifice contraction.

2.4 Boundary Condition

The boundary conditions were defined to represent the internal flow through the pipe and the orifice as accurately as possible. At the inlet, a uniform velocity profile was imposed to prescribe the required flow rate for each Reynolds number investigated. The inlet velocity $\mathrm{U}_{\mathrm{in}}$was calculated using the Reynolds number relation for incompressible flow,

$$Re = \frac{\rho U_{in} D}{\mu} \tag{5}$$

where D is the inlet diameter, ρis the fluid density, and μ is the dynamic viscosity. This ensures that each simulation corresponds to the intended flow regime [10].

A static pressure condition was applied at the outlet to allow the fluid to exit the domain freely. The gauge pressure at the outlet was set to zero, expressed as:

$$p_{out} = 0 \tag{6}$$

This condition enables the solver to determine the natural pressure field produced by the flow constriction and is used in computing the pressure difference across the orifice [11]. The no slip condition was applied at all pipe walls, enforcing zero velocity at the solid boundaries. This is written as:

$$\vec{u} = 0 \text{ at the wall} \tag{7}$$

which is essential for accurately modelling viscous effects and wall shear stresses. For simulations involving turbulence models, turbulence quantities at the inlet were assigned based on standard internal flow recommendations [12]. The turbulent kinetic energy $k$and turbulent dissipation rate εwere estimated using:

$$k = \frac{3}{2}(U_{in}I)^2 \tag{8}$$

$$\varepsilon = C_{\mu}^{3/4}\frac{k^{3/2}}{L} \tag{9}$$

where I is the turbulence intensity, C_{μ} is a model constant, and L is the turbulence length scale. These values provided stable initialization for all turbulence models used in the study.

Together, these boundary conditions ensured a realistic and physically consistent representation of the flow through the orifice, allowing the solver to accurately evaluate velocity distributions, pressure fields, and overall flow behaviour [13].

2.5 Analysis

2.5.1 Velocity analysis

The velocity distribution within the flow domain was evaluated using the numerical results obtained from the CFD simulation. Velocity analysis is essential for understanding how fluid accelerates and decelerates as it moves through the geometry, as well as for validating the simulation against theoretical expectations. The computed velocity field allows for the identification of regions of high and low velocity magnitude, which provides insights into flow behavior such as acceleration near the inlet, uniformity within the test section, and changes in flow characteristics toward the outlet.

For incompressible fluid flow, velocity is governed by the continuity equation:

$$\nabla \cdot \vec{V} = 0 \tag{10}$$

where $\vec{V}$ is the velocity vector [14, 15]. This equation ensures that mass is conserved throughout the computational domain. The velocity field is also influenced by the momentum equation, expressed as:

$$\rho\left(\frac{\partial\vec{V}}{\partial t}+\vec{V}\cdot\nabla\vec{V}\right)=-\nabla p+\mu\nabla^{2}\vec{V} \tag{11}$$

where ρ is the density, $p$is the static pressure, and μ is the dynamic viscosity of air [16]. Under steady state conditions with negligible body forces, the left side reduces to the convective acceleration term, indicating that velocity changes are primarily due to pressure gradients and viscous effects.
Velocity magnitude in the simulation was calculated using:

$$V_{\text{mag}}=\sqrt{u^{2}+v^{2}+w^{2}} \tag{12}$$

where u, v, and $w$represent the velocity components in the three coordinate directions. This quantity allows for the visualization of overall flow acceleration and is used to compare the performance of different turbulence models. The resulting velocity profiles provide quantitative information needed to assess whether the flow inside the duct reaches a fully developed condition and whether the model predictions align with theoretical expectations and past literature [17].

2.5.2 Pressure analysis

Pressure analysis was conducted to evaluate the pressure distribution along the pipe and across the orifice contraction. Pressure is a key parameter in internal flow studies because it governs fluid acceleration and energy conversion as the flow encounters geometric changes. In this study, the pressure field obtained from the CFD simulation was used to determine the pressure difference between the inlet and outlet, which serves as an indicator of fluid resistance and flow losses caused by the orifice. The pressure behaviour in incompressible flow is governed by the steady form of the Navier Stokes equation.

$$\rho\left(\vec{V}\cdot\nabla\vec{V}\right)=-\nabla p+\mu\nabla^{2}\vec{V} \tag{13}$$

which shows that pressure gradients directly contribute to the acceleration or deceleration of the fluid [18]. As the flow passes through the orifice opening, conservation of mass requires the velocity to increase, and according to Bernoulli’s principle, this results in a local reduction in static pressure. Downstream of the orifice, the flow expands, decelerates, and experiences a pressure recovery region. However, due to viscous losses and flow separation, full recovery does not occur, and a measurable pressure drop remains. The pressure difference across the orifice was calculated using:

$$\Delta p=p_{\text{inlet}}-p_{\text{outlet}} \tag{14}$$

where $p_{\text{inlet}}$is the static pressure at the inlet and $p_{\text{outlet}}$is the static pressure at the exit section [19]. This value was used as a quantitative parameter to compare the effects of different mesh resolutions, Reynolds numbers, and turbulence models. Areas of high adverse pressure gradient were also identified to analyze the tendency of the flow to separate downstream of the contraction.

The pressure contours and line plots generated from the CFD results provided a detailed representation of the pressure behaviour throughout the domain. These data allow for verification of numerical accuracy and help establish the relationship between geometry induced acceleration, energy loss, and turbulence effects in the pipe flow [20].

3. Results

3.1 Grid Independence Test Results

To make sure that the numerical findings from the simulation matched physically valid flow behaviour and were not affected by mesh size, a grid independence test was carried out. Under the same boundary conditions, three meshes with different resolutions, coarse (20 mm), medium (10 mm), and fine (5 mm) were created and tested. From 3,801 elements in the coarse mesh to 20,032 elements in the fine mesh, the number of elements increased dramatically during the course of the three scenarios. This methodical improvement made it possible to thoroughly assess how mesh density affects important output factors like maximum velocity and pressure distribution throughout the pipe with the contraction.

The findings gathered in Table 4 demonstrates that, with only minor variations noted, maximum velocity stayed comparatively constant across the three mesh types. A velocity of 8.244 m/s was achieved by the coarse mesh, 8.261 m/s by the medium mesh, and 8.137 m/s by the small mesh. Further refinement beyond 10 mm element size results in relatively slight variations in anticipated velocity, as evidenced by the little discrepancy between the medium and fine mesh. A similar pattern was seen in the maximum inlet pressure, which increased slightly from 36.57 Pa in the coarse mesh to 37.41 Pa in the fine mesh. Figure 3 shows slight variations imply that mesh density has little bearing on velocity forecasts at the orifice.

The maximum outlet pressure showed the biggest difference. The coarse and medium meshes displayed values of 0.003489 Pa and 0.004201 Pa, respectively, while the fine mesh displayed a significantly higher value of 0.09111 Pa. This increase can be explained by the fine mesh's enhanced capacity to capture the tiny but significant pressure changes that coarser meshes tend to smooth out, as well as the flow gradients and recirculation zones downstream of the contraction. Despite this discrepancy, the medium and fine meshes exhibited similar overall flow properties, including the velocity behaviour and general pressure trends.

Table 4
Grid independency test results

Mesh type	Number of elements	Maximum velocity (m/s)	Max inlet pressure (Pa)	Difference in pressure (Pa)
Coarse (20 mm)	3801	8.244	36.57	0.003489
Medium (10 mm)	4864	8.261	37.02	0.004201
Fine (5 mm)	20032	8.137	37.41	0.09111

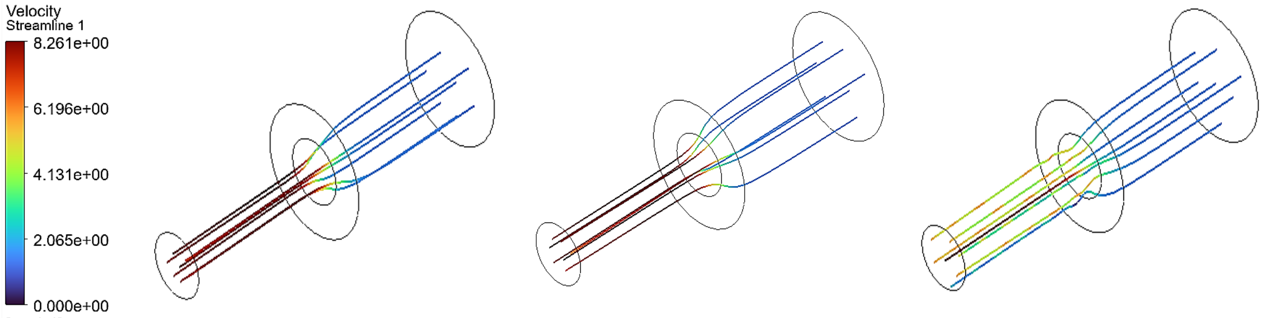

(a) (b) (c)

Fig. 3. Velocity profiles (a) Coarse (b) Medium (c) Fine

Based on these findings, the medium mesh (10 mm), which provides a good compromise between computational cost and solution accuracy, is deemed accurate enough for more runs. The little variations between the medium and fine mesh verify that the primary flow parameters of concern are not substantially affected by mesh refinement above the medium resolution. For the rest of the investigation, the medium mesh grid is chosen since it is considered grid independent.

3.2 Velocity Results for Variation in Geometry

The geometry variation test results in Table 5 shows that changes in the internal geometry produced noticeable effects on the maximum velocity within the flow domain. Design 1 recorded a peak velocity of 8.213 metres per second, while Design 2 exhibited a slightly lower value of 7.819 metres per second. Design 3 produced the highest velocity at 8.496 metres per second. These variations indicate that subtle differences in geometry influence the acceleration of the fluid, with Design 3 providing the most streamlined flow path that enhances fluid speed. Overall, the results in Figure 4 demonstrates that geometric optimisation plays a significant role in controlling velocity distribution in internal flow systems.

Table 5
Geometry variation test results for velocity

Designs	Max velocity (m/s)
Design 1	8.213
Design 2	7.819
Design 3	8.496

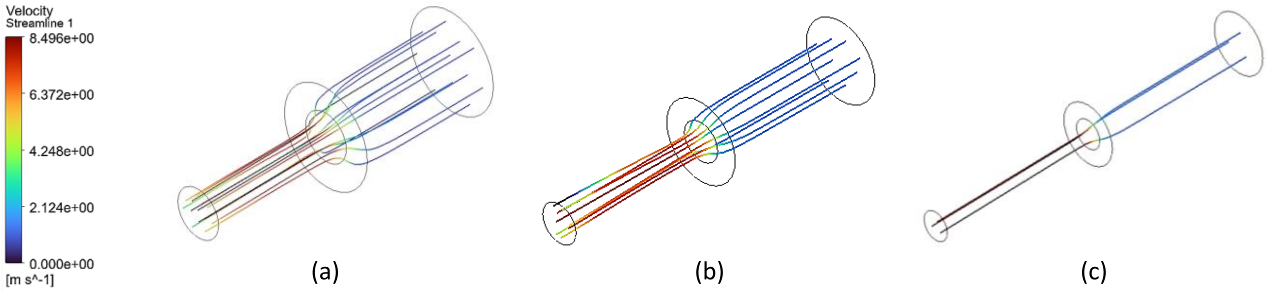

(a) (b) (c)

Fig. 4. Design of geometry (a) Design 1 (b) Design 2 (c) Design 3

3.3 Velocity Results for Variation in Turbulence Models

Three popular turbulence models, the Standard k-ε, the Realizable k-ε, and the k-ωSST model, were used to assess the impact of turbulence modelling on the precision of the CFD predictions. When it comes to forecasting flow separation, near-wall behaviour, and shear-layer growth surrounding the contraction region, each model has varying strengths. This study as gathered in Table 6 evaluates how well these models capture important flow phenomena such jet contraction, recirculation zones, and pressure recovery downstream of the orifice-like constriction by comparing velocity contours, pressure fields, and centreline profiles.

The flow behaviour is sensitive to the choice of turbulence modelling, as seen by the results of the analysis of the flow through the system using several turbulence models, which show modest differences in both velocity and pressure characteristics. The greatest velocity recorded for the standard k-ε model was 8.213 m/s, and the corresponding maximum inlet pressure was 37.10 Pa. For this model, the pressure distribution along the flow path was almost uniform since the outlet pressure difference, which represents the change from the inlet, was negligible at 0.008765 Pa. This implies that a somewhat higher peak velocity with little pressure loss over the outflow is predicted by the k-ε model.

By contrast, the k-ω model yielded a maximum inlet pressure of 35.56 Pa and a somewhat lower maximum velocity of 7.854 m/s. Even while it is still little, the resulting outlet pressure difference climbed to 0.01503 Pa, which is about twice as much as the difference seen with the k-ε model. This suggests that a somewhat different momentum and turbulence distribution throughout the domain is reflected in the k-ω model, which predicts a more pronounced pressure drop along the flow route coupled with a slightly lower maximum velocity.

Table 6
Turbulence models test results

Turbulence models	Max velocity (m/s)	Max inlet pressure (Pa)	Difference in outlet pressure (Pa)
$k - \epsilon$	8.213	37.10	0.008765
$k - \omega$	7.854	35.56	0.01503
Realizable $k - \omega$	7.791	35.57	0.02897

Overall findings in Figure 5 highlights the fact that, despite the fact that all three turbulence models predict comparable general flow patterns, there are noticeable variations in the distribution of pressure and velocity. While both k-ω models reflect ever larger pressure changes and lower velocities, with the realizable k-ω exhibiting the greatest variance, the k-ε model tends to forecast slightly higher velocities and more uniform pressures. These differences highlight how crucial it is to choose the right turbulence model based on the required level of precision for the system's velocity and pressure forecasts.

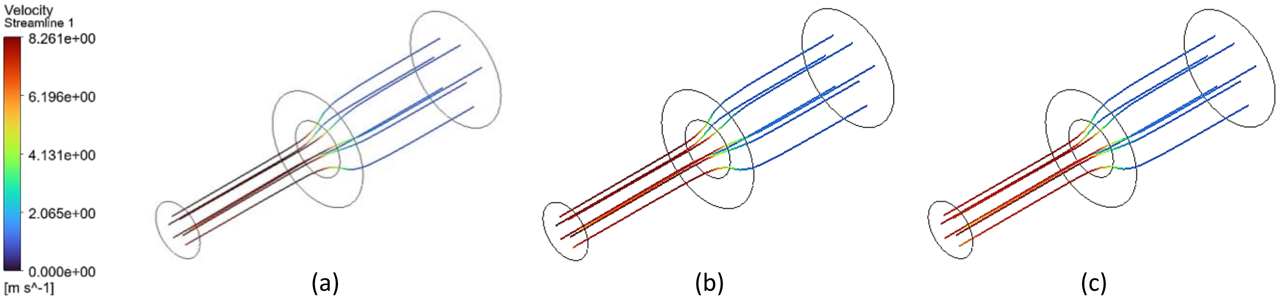

(a) (b) (c)

Fig. 5. (a) $k - \epsilon$ (b) $k - \omega$ (c) Realizable $k - \omega$

3.4 Velocity Results for Variation in Reynolds Numbers

Distinct differences in the velocity distribution and pressure behaviour throughout the pipe's contraction and outflow sections when the three Reynolds number regimes, laminar, transitional, and turbulent, in Table 7 are analysed. The smooth and well-organized flow profile was reflected in the laminar case's maximum velocity of 7.933 m/s. The laminar flow lost very little energy and maintained almost the same pressure levels at both borders, as evidenced by the pressure differential of 0 Pa between the inlet and output. The development of flow instabilities and partial mixing caused the maximum velocity to rise to 8.213 m/s as the flow entered the transitional regime. As the flow became less regular, this regime produced a little inlet - outlet pressure difference of 0.008765 Pa, indicating slight losses.

Due to strong mixing and a more complete velocity profile as shown in Figure 6, the maximum velocity in the turbulent domain was 8.261 m/s, the highest of the three. While turbulence increases momentum transfer, the energy distribution through the core region leads in a smaller pressure drop across the outlet, as seen by the corresponding pressure differential of 0.004201 Pa, which is marginally lower than the transitional case. In general, as the flow changes from laminar to totally turbulent behaviour, an increase in Reynolds number results in higher velocities and slight but significant changes in pressure differential.

Table 7
Reynold’s numbers test results

Reynold’s numbers	Max velocity (m/s)	Max inlet pressure (Pa)	Difference in pressure (Pa)
Laminar	7.933	33.88	0 (Shows that it is similar to inlet pressure)
Transitional	8.213	37.10	0.008765
Turbulent	8.261	37.02	0.004201

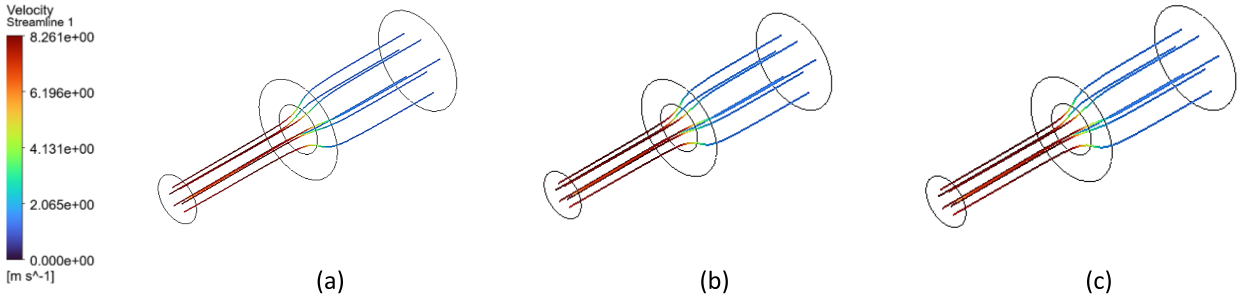

(a) (b) (c)

Fig. 6. (a) Laminar (b) Transitional (c) Turbulent

3.5 Pressure Results for Variation in Geometry

The pressure analysis for the three pipe geometries with sudden contraction shows that each configuration influences the inlet pressure and the resulting pressure difference across the contraction (Table 8). Design 1 recorded a maximum inlet pressure of 37.10 Pa with the lowest pressure difference (0.008765 Pa), indicating comparatively lower flow resistance. Design 2 exhibited a slightly lower inlet pressure of 36.32 Pa but produced a higher-pressure difference of 0.01570 Pa, suggesting increased local energy losses.

Design 3 showed the highest inlet pressure at 41.13 Pa and the greatest pressure difference (0.02225 Pa), demonstrating that its geometry introduces the most significant flow disturbance at the contraction. Overall, the results indicate that small geometric variations can noticeably affect pressure behaviour, with more abrupt or restrictive designs generating higher losses and greater pressure fluctuations.

Table 8
Geometry variation test results for pressure

Designs	Max inlet pressure (Pa)	Difference in pressure (Pa)
1	37.10	0.008765
2	36.32	0.01570
3	41.13	0.02225

3.6 Pressure Results for Variation in Turbulence Models

Table 9 shows that at a maximum inlet pressure of 35.57 Pa, the realizable k-ω model produced the lowest maximum velocity of the three models, at 7.791 m/s. A more noticeable pressure change in comparison to the intake is suggested by the outlet pressure differential, which climbed to 0.02897 Pa. This behaviour shows that the realizable k-ω model, which was created to better capture complex flow characteristics like strong streamline curvature or separation, predicts a slightly higher kinetic energy dissipation along the flow path, which leads to the highest-pressure difference at the outlet and the lowest peak velocity.

Table 9
Results of turbulence model's test

Turbulence models	Max inlet pressure (Pa)	Difference in outlet pressure (Pa)
$k-\epsilon$	37.10	0.008765
$k-\omega$	35.56	0.01503
Realizable $k-\omega$	35.57	0.02897

3.7 Pressure Results for Variation in Reynolds Numbers

The pressure results obtained for different Reynolds number regimes which are laminar, transitional, and turbulent to demonstrate how flow behaviour influences the pressure distribution across the orifice is shown in Table 10. Under laminar conditions, the maximum inlet pressure was 33.88 Pa, and the pressure difference was effectively zero, indicating minimal energy loss and a nearly uniform pressure between the inlet and outlet. This is expected, as laminar flow is dominated by orderly fluid motion with limited disturbance around the orifice.

In contrast, both transitional and turbulent flows exhibited higher inlet pressures of 37.10 Pa and 37.02 Pa respectively, along with measurable pressure differences. The transitional regime recorded the highest-pressure difference at 0.008765 Pa, followed by the turbulent regime at 0.004201 Pa. These increases reflect the greater flow instability and enhanced mixing that occur as the Reynolds number rises, leading to more pronounced pressure drops across the orifice. Overall, the results show that pressure losses increase when the flow shifts away from laminar behaviour, with transitional flow producing the most significant variation in this study.

Table 10
Results of Reynold's numbers test

Reynold's numbers	Max inlet pressure (Pa)	Difference in pressure (Pa)
Laminar	33.88	0 (Shows that it is similar to inlet pressure)
Transitional	37.10	0.008765
Turbulent	37.02	0.004201

4. Conclusions

This study's CFD analysis effectively illustrates how pipe shape, constriction ratio, and turbulence modelling affect the resulting pressure and velocity distributions in an internal flow system. Reducing the inlet and outlet sizes resulted in higher maximum velocities and larger outlet pressure differences, a consistent and physically coherent trend was seen throughout the three geometries examined. With a D1 of 50 mm and a D2 of 25 mm, the smallest geometry (Design 3) generated the largest pressure difference and peak velocity of 8.496 m/s, suggesting increased acceleration and energy dissipation through the small orifice. Conversely, the largest shape (Design 1) maintained moderately high velocities and lower pressure losses, indicating less contraction effects and smoother flow transitions. The continuity and Bernoulli equations, in particular, which anticipate velocity amplification and pressure reduction in response to decreased flow area, are in good agreement with these behaviours. In addition, the inlet pressure increased by roughly 9-10% when comparing laminar to transitional flow conditions, while the turbulent regime exhibited about 50%

lower pressure difference than the transitional regime, further validating the influence of flow regime on orifice-induced losses.

Complementary simulations with the k–ε, k–ω, and realizable k–ω turbulence models further demonstrated that all models consistently represented the expected flow behaviour, despite minor differences in predicted velocity and pressure. This supports the simulation framework's dependability and verifies that the reported outcomes are representative of real flow physics rather than numerical artifacts. The findings' validity is reinforced by their uniformity across turbulence models.

The results' validity is further reinforced by comparison with existing literature. Research on abrupt contractions and sharp-edged orifices repeatedly shows that when the diameter ratio drops, local flow velocities rise in tandem with increases in pressure-loss coefficients and differential pressure. The project's observed trends align with these empirically proven correlations, and the pressure change magnitudes fall within ranges documented in earlier studies that dealt with low static pressure circumstances and moderate input velocities. Strong proof of the accuracy and validity of the CFD predictions is provided by the agreement between the simulated behaviour and published experimental data.

Overall, the study accomplishes its goals by demonstrating how geometric scaling influences important flow characteristics and by confirming that the CFD results are solidly supported by both previous research findings and fluid mechanics theory. The alignment between the numerical outcomes, theoretical expectations, and literature benchmarks clearly indicates that the objectives of analysing mesh effects, Reynolds number behaviour, and turbulence model performance have been fully achieved. The findings offer a solid basis for pipe-orifice arrangement optimization in the future, especially in applications requiring targeted velocity amplification or controlled pressure drop.

References

[1] Nygård, F., and H. I. Andersson. "Numerical simulation of turbulent pipe flow through an abrupt axisymmetric constriction." *Flow, Turbulence and Combustion* 91, no. 1 (2013): 1-18. https://doi.org/10.1007/s10494-013-9447-y

[2] ISO, EN. "5167-2: Measurement of fluid flow by means of pressure differential devices inserted in circular cross-section conduits running full." *International Organization for Standardization, Switzerland* (2003).

[3] Karthik, G. S. Y., K. J. Kumar, and V. Seshadri. "Prediction of performance characteristics of orifice plate assembly for non-standard conditions using CFD." Int. J. Eng. Tech. Res 3, no. 5 (2015): 162-167.

[4] Barki, Malatesh, T. Ganesha, and M. C. Math. "CFD analysis and comparison of fluid flow through a single hole and multi hole orifice plate." International Journal of Research in Advent Technology 2, no. 8 (2014): 6-15.

[5] Rashid, Farhan Lafta, Haider Nadhom Azziz, and Emad Qasem Hussein. "An analytical and numerical investigation of pressure drop and velocity distribution in obstructed tube." *Advances in Natural and Applied Sciences* 10, no. 11 (2016): 140-149.

[6] Araoye, Abdulrazaq A., Hasan M. Badr, and Wael H. Ahmed. "Investigation of flow through multi-stage restricting orifices." *Annals of Nuclear Energy* 104 (2017): 75-90. https://doi.org/10.1016/j.anucene.2017.02.002

[7] Martins, Nuno MC, Dídia IC Covas, Silvia Meniconi, Caterina Capponi, and Bruno Brunone. "Characterisation of low-Reynolds number flow through an orifice: CFD results vs. laboratory data." *Journal of Hydroinformatics* 23, no. 4 (2021): 709-723. https://doi.org/10.2166/hydro.2021.101

[8] Gronych, T., M. Jeřáb, L. Peksa, J. Wild, F. Staněk, and M. Vičar. "Experimental study of gas flow through a multi-opening orifice." *Vacuum* 86, no. 11 (2012): 1759-1763. https://doi.org/10.1016/j.vacuum.2012.02.008

[9] Haimin, Wang, Xie Shujuan, Sai Qingyi, Zhou Caimin, Lin Hao, and Chen Eryun. "Experiment study on pressure drop of a multistage letdown orifice tube." *Nuclear Engineering and Design* 265 (2013): 633-638. https://doi.org/10.1016/j.nucengdes.2013.09.014

[10] Hollingshead, Colter L., Michael C. Johnson, Steven L. Barfuss, and Robert E. Spall. "Discharge coefficient performance of Venturi, standard concentric orifice plate, V-cone and wedge flow meters at low Reynolds

numbers." *Journal of Petroleum Science and Engineering* 78, no. 3-4 (2011): 559-566. https://doi.org/10.1016/j.petrol.2011.08.008

[11] Ramamurthi, Krishnaswami, and K. Nandakumar. "Characteristics of flow through small sharp-edged cylindrical orifices." *Flow measurement and Instrumentation* 10, no. 3 (1999): 133-143. https://doi.org/10.1016/S0955-5986(99)00005-9

[12] Muñoz-Díaz, Enrique, Francisco J. Solorio-Ordaz, and Gabriel Ascanio. "A numerical study of an orifice flowmeter." *Flow Measurement and Instrumentation* 26 (2012): 85-92. https://doi.org/10.1016/j.flowmeasinst.2012.03.012

[13] Rani, H. P., T. Divya, R. R. Sahaya, V. Kain, and D. K. Barua. "Numerical investigation of energy and Reynolds stress distribution for a turbulent flow in an orifice." *Engineering Failure Analysis* 34 (2013): 451-463. https://doi.org/10.1016/j.engfailanal.2013.08.010

[14] Shaaban, S. "Optimization of orifice meter's energy consumption." *Chemical engineering research and design* 92, no. 6 (2014): 1005-1015.

[15] Shah, Manish S., Jyeshtharaj B. Joshi, Avtar S. Kalsi, C. S. R. Prasad, and Daya S. Shukla. "Analysis of flow through an orifice meter: CFD simulation." *Chemical Engineering Science* 71 (2012): 300-309.

[16] Shih, Tsan-Hsing, William W. Liou, Aamir Shabbir, Zhigang Yang, and Jiang Zhu. "A new k-ϵ eddy viscosity model for high reynolds number turbulent flows." Computers & Fluids 24, no. 3 (1995): 227-238. https://doi.org/10.1016/0045-7930(94)00032-T

[17] Shan, Feng, Atsushi Fujishiro, Tatsuya Tsuneyoshi, and Yoshiyuki Tsuji. "Effects of flow field on the wall mass transfer rate behind a circular orifice in a round pipe." *International Journal of Heat and Mass Transfer* 73 (2014): 542-550. https://doi.org/10.1016/j.ijheatmasstransfer.2014.02.039

[18] Sridevi, T., Dhana Sekhar, and V. Subrahmanyam. "Comparison of flow analysis through a different geometry of flowmeters using fluent software." *International Journal of Research in Engineering and Technology* 3, no. 08 (2014): 141-149. https://doi.org/10.15623/ijret.2014.0308023

[19] Vemulapalli, Sravani, and Santhosh Krishnan Venkata. "Parametric analysis of orifice plates on measurement of flow: A review." Ain Shams Engineering Journal 13, no. 3 (2022): 101639. https://doi.org/10.1016/j.asej.2021.11.008

[20] Zahariea, D. "Numerical analysis of eccentric orifice plate using ANSYS Fluent software." In IOP Conference Series: Materials Science and Engineering, vol. 161, no. 1, p. 012041. IOP Publishing, 2016. https://doi.org/10.1088/1757-899X/161/1/012041